Perspective

2D MOFs and Zeolites for Composite Membrane and Gas Separation Applications: A Brief Review

Published as part of ACS Materials Au virtual special issue "2023 Rising Stars".

Minsu Kim, Wooyoung Choi, Choong Hoo Lee, and Dae Woo Kim*

Cite This: *ACS Mater. Au* 2024, 4, 148−161

Read Online

ACCESS | Metrics & More | Article Recommendations

ABSTRACT: Commercial membranes have predominantly been fabricated from polymers due to their economic viability and processability. This choice offers significant advantages in energy efficiency, cost-effectiveness, and operational simplicity compared to conventional separation techniques like distillation. However, polymeric membranes inherently exhibit a trade-off between their permeability and selectivity, which is summarized in the Robeson upper bound. To potentially surpass these limitations, mixed-matrix membranes (MMMs) can be an alternative solution, which can be constructed by combining polymers with inorganic additives such as metal−organic frameworks (MOFs) and zeolites. Incorporating high-aspect-ratio fillers like MOF nanosheets and zeolite nanosheets is of significant importance. This incorporation not only enhances the efficiency of separation processes but also reinforces the mechanical robustness of the membranes. We outline synthesis techniques for producing two-dimensional (2D) crystals (including nanocrystals with high aspect ratio) and provide examples of their integration into membranes to customize separation performances. Moreover, we propose a potential trajectory for research in the area of high-aspect-ratio materials-based MMMs, supported by a mathematical-model-based performance prediction.

KEYWORDS: 2D materials, high aspect ratio, metal−organic frameworks, zeolites, composite membrane, gas separation
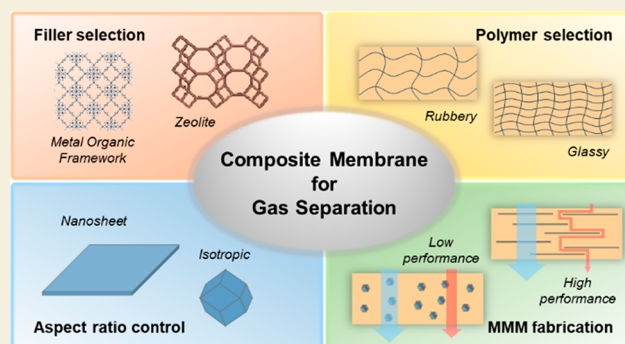
INTRODUCTION

Membrane separation technology has been widely used in various industrial applications, including water treatment, pharmaceuticals, food and beverage, petrochemicals, and more.[1] Mainly for gas separations, membranes are used in various processes to separate different kinds of gases, including carbon dioxide capture, ammonia separation, natural gas sweetening, hydrogen separation, syngas production, dehydration, and hydrocarbon separations in petrochemical areas.[2,3] Membrane separation technology is expected to offer energy-efficient, cost-effective, and environmentally friendly separation solutions in various industries, benefiting from compact design, ease of operation, and scalability.[4,5]

Polymers are predominantly employed as membrane materials due to their cost-effectiveness and moderate selectivity, but they exhibit a permeability−selectivity trade-off known as the Robeson upper bound.[6] To address this limitation, ongoing research explores diverse polymer modifications.[7,8] A promising approach involves incorporating filler materials, resulting in composite membranes, so-called mixed-matrix membranes (MMMs).[9,10] These composite membranes consist of a polymer matrix integrated with fillers like metal−organic frameworks (MOFs) and zeolite nano/microparticles. The

strategic combination of these porous materials with high permeability and selectivity holds the potential to surpass the upper bound and achieve commercially appealing outcomes.

Even with the aforementioned advantages, in conventional MMMs it is challenging to achieve strong compatibility between the polymer matrix and the incorporated filler materials.[11] Ensuring proper dispersion and adhesion of these fillers within the polymer matrix is complex, potentially leading to low separation performance with reduced mechanical stability. If not properly managed, poor compatibility can result in filler agglomeration, inadequate interface bonding, and rearrangement of polymer chains on the surface of the fillers. Consequently, consistent and reliable MMM performance can only be achieved through material selection, precise fabrication techniques, and comprehensive characterization.
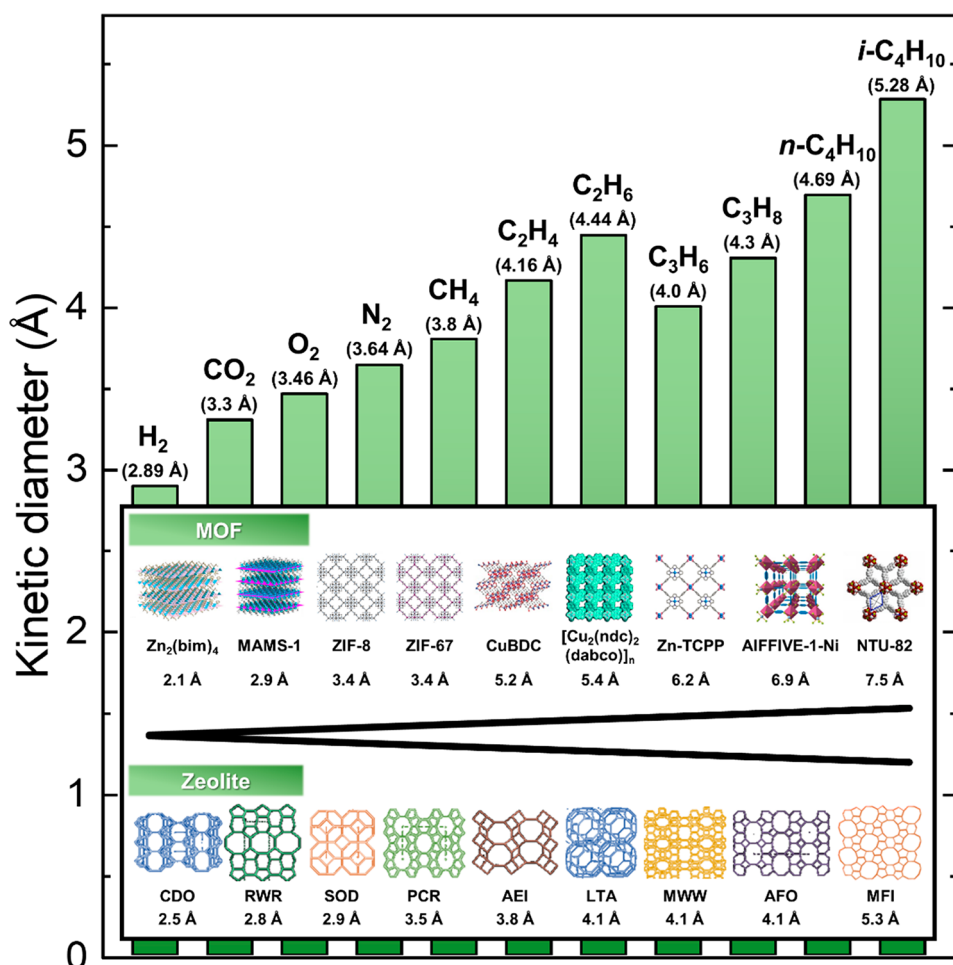
Figure 1. Kinetic diameters of industrially important gas molecules and examples of MOF and zeolite crystal types prepared in the form of nanosheets or plates with high aspect ratio.

On the other hand, performance enhancement can be maximized when high-aspect-ratio fillers such as zeolite nanosheets and MOF nanosheets are used instead of isotropic particles.[12] The high-aspect-ratio fillers are known for offering tortuous pathways, particularly for nonpermeable molecules.[13] At the same time, permeable gas can easily permeate through the composite membranes, which can significantly enhance gas selectivity based on diffusion pathway difference. Moreover, two-dimensional (2D) fillers can improve mechanical strength, such as stiffness and modulus, allowing MMM fabrication with high-loading fillers.[14,15] The layered structure of 2D fillers can decrease the occurrence of defects and imperfections compared to isotropic particles. Consequently, this feature enhances the uniformity and predictability of separation performance. Furthermore, the integration of a 2D filler allows for the fabrication of a thin coating layer on porous supports, thereby reducing the overall thickness of the resulting membrane, which is required for preparing practical unsymmetric composite membranes.[16]

Within this perspective, we focus on 2D MOFs and 2D zeolites that have been prepared in powder form to explore their potential for integration into composite membranes. Our objective is to present techniques for synthesizing 2D crystals and to elucidate their incorporation into membranes, specifically targeting gas separation applications. We also propose a forward-looking trajectory for research into MMMs based on 2D

materials, supported by the implementation of a mathematical model.

■ PREPARATION OF 2D MOF AND 2D ZEOLITE NANOSHEETS

Recognized as the pioneer among various 2D materials, graphene possesses atomic thickness and a high aspect ratio, rendering it a suitable candidate for polymer composites.[17] Nonetheless, graphene's intrinsic gas barrier properties make it unsuitable for direct implementation in gas separation applications.[18,19] For the graphene prepared by chemical vapor deposition (CVD), pore generation is achievable to enhance separation performance for specific gases.[20] However, the CVD graphene is prepared as a thin film and requires a transfer process from metal foils to porous supports.[21,22] More importantly, challenges persist in generating powdered porous graphene and facilitating its integration with polymers. The resultant pores, furthermore, exhibit limitations in their capacity for distinct gas segregation. Pore generation of graphene oxide via post-treatment, including chemical reduction and thermal activation, is a relatively easy way to prepare nanoporous graphene powder; however, it is difficult to precisely define and control the pore size and density.[23,24] Ideally, developing materials with atomically controlled porous crystals, such as MOFs and zeolites, in 2D configurations holds promise for circumventing these challenges because the difference in the
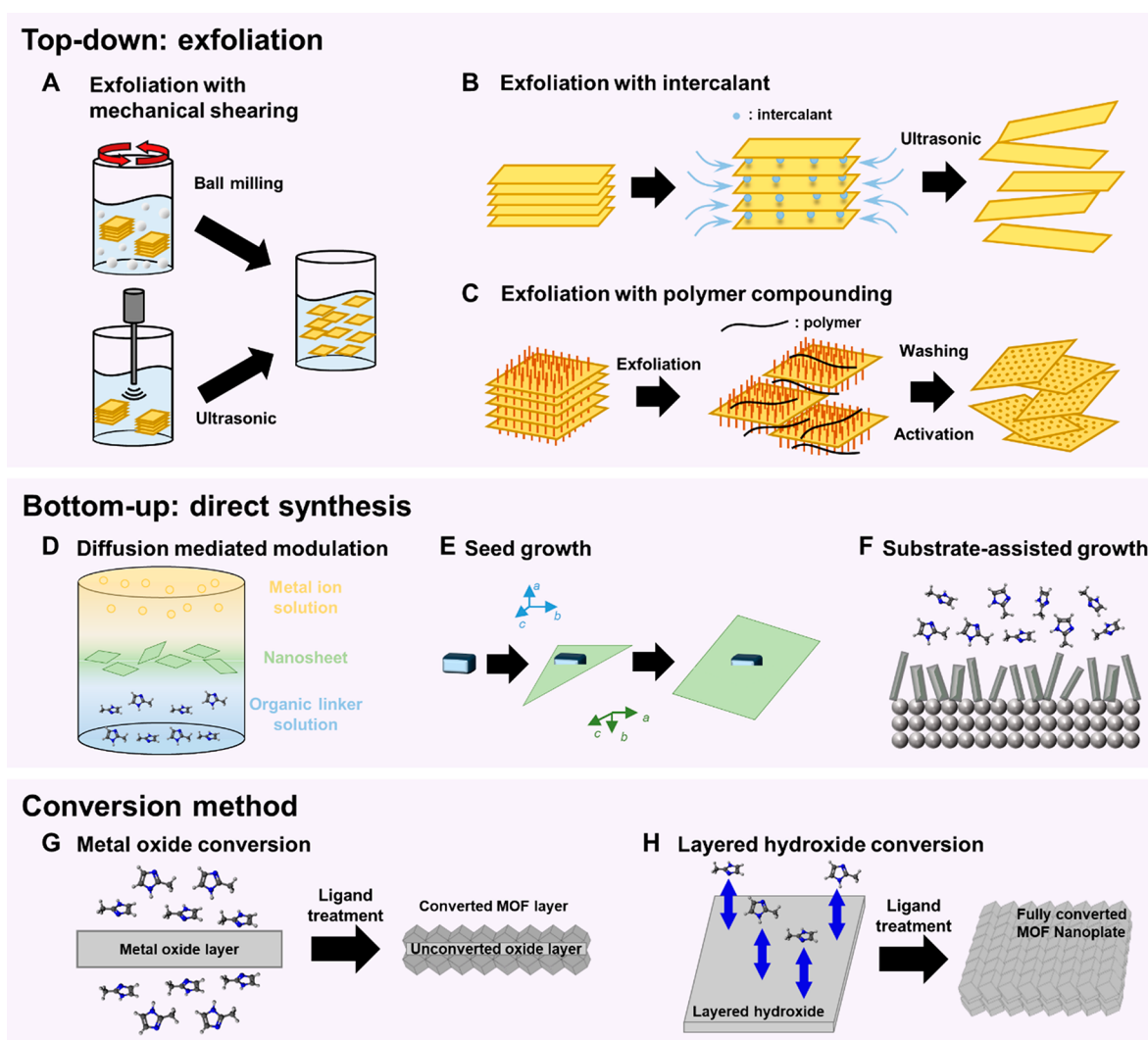
Figure 2. Preparation methods of MOF and zeolite nanosheets.

kinetic sizes of gas molecules is tiny, from a few angstroms to subangstrom levels. Therefore, porous crystals with precisely controlled pore sizes are necessary for effective separation.

The Cambridge Structural Database and the International Zeolite Association Structure Commission (IZA-SC) collectively list over 120,000 crystal structures for MOFs and 255 crystal structures for zeolites, but only a few have been successfully synthesized and applied, typically in isotropic particle shapes.[25,26] Recognizing the advantages conferred by 2D nanosheets, such as substantial surface area, elevated surface-to-volume atom ratio, and reduced diffusion paths, intensive efforts are directed toward the 2D synthesis of MOFs and zeolites. Notably, only a few 2D MOF and zeolite nanosheets have been prepared in powder form (Figure 1). A subset of these crystals possesses pore apertures positioned between specific gas molecules, enabling size-based molecular separation. Notable examples include the SOD-type zeolite and MAMS-1 utilized for H_2/CO_2 separation and the deployment of ZIF-67 for CO_2/N_2 separation.[27,28] However, certain crystals like copper 1,4-benzenedicarboxylate (CuBDC) and MWW zeolite, with aperture sizes of 5.2 and 4.1 Å, respectively, characterized by larger aperture dimensions relative to typical gas molecules, find application in compact gas separations like H_2/CO_2 and CO_2/N_2.[29−31] This is attributed to separation mechanisms extending

beyond molecular sieving, as gas−crystal interactions significantly influence permeation dynamics.[32,33] In contrast to smaller gas molecules like H_2 or CO_2, the utilization of 2D nanosheets to separate relatively larger gas molecules such as hydrocarbons has been rarely reported. A distinctive instance is observed with MFI-type (or MFI/MEI-type) zeolite nanosheets, showcasing notable efficacy in separating xylene isomers and in butane isomer separation.[34] To achieve the separation of diverse and economically essential gas molecules, it is required to precisely tailor the pore aperture dimensions of MOFs and zeolites as well as to couple them with reliable membrane fabrication techniques.

The preparation method of those 2D MOFs and zeolites (or high-aspect-ratio nanoplates) can be divided into three big categories: top-down exfoliation, bottom-up direct synthesis, and conversion methods (Figure 2). Just as the solution-phase exfoliation of graphene from graphite has been documented in initial studies on 2D materials, the exfoliation of nanosheets from larger particles has been observed in the case of MOFs and zeolites since their earliest investigations.[30,35,36] This phenomenon arises due to the presence of an interlayer structure and stacking of layers within certain crystal structures of MOFs and zeolites. Particularly with zeolites, the structural configuration frequently involves organic compounds, like alkyl chains, being

incorporated between zeolite sheets of the unit cell's dimensions, a characteristic influenced by the type of structure-directing agent (SDA).[37−39]

Mechanical exfoliation, such as ball milling and ultrasonication, involves the delamination of bulk MOFs or zeolite crystals into 2D nanosheets by applying shear force (Figure 2A).[40,41] By controlled mechanical stress, layers are separated from parent crystals. Bulk crystals are pulverized into fine sheets using balls within a rotating container in ball milling. Ultrasonication employs high-frequency sound waves that can fracture the bulk crystal's layers. Peng et al. proposed a physical exfoliation process to synthesize $Zn_2(bim)_4$ nanosheets.[40] Pristine bulk crystals were first ball-milled and then ultrasonicated in volatile solvent to obtain 1.12 nm thickness nanosheets. The $Zn_2(bim)_4$ membrane on a porous support exhibited H_2 permeance of 2700 GPU with H_2/CO_2 selectivity of 291. Both methods are feasible for synthesizing small amounts of 2D nanosheets but unsuitable for large-scale production. Moreover, the in-plane structure can be damaged due to the physical force, and the lateral size can decrease.

Interlayer intercalation is an exfoliation method that is based on introducing guest molecules, typically ions, solvents, or polymers, into the interlayer spaces of layered MOFs or zeolite bulk particles (Figure 2B).[42,43] These intercalants induce subsequent swelling of the layers, which facilitates delamination. Ding et al. demonstrated the synthesis of $Zn_2(PdTCPP)$ nanosheets by chemical exfoliation from the intercalation method.[42] Due to the intercalation of the dipyridyl ligand, the interlayer interactions between nanosheets of the parent bulk crystal are weakened, resulting in the exfoliation of subnanometer nanosheets in high yield. This method can yield significant quantities of 2D nanosheets, but additional steps might be necessary to eliminate intercalants from the final product.

The polymer compounding method blends bulk material with a polymer and induces shear force to divide bulk crystals into layers (Figure 2C).[34,37] The polymer can stabilize the exfoliated nanosheets and prevent them from aggregating or restacking. The Tsapatsis and Agrawal groups reported the polymer compounding method for the exfoliation of MWW and MFI zeolite nanosheets.[44] Layered precursors were melt-blended with polystyrene and compounded with a twin-screw extruder. The obtained nanosheet−polymer nanocomposites were dispersed in a solvent and sonicated. Finally, larger particles were removed by centrifugation. Despite the fact that the process can prepare nonaggregated intact nanosheets, the viscosity of the polymer matrix and shear force can significantly influence the effectiveness, and the processing steps are laborious because the polymer must be removed from the final product with solvent washing. In addition, for polymer composites, the zeolite nanosheets must be calcined at a high temperature of around 500 °C or employed with a reactive solvent (piranha solution) to remove the SDA molecules.[34,39,45]

Diffusion-mediated modulation is a synthesis method of 2D MOF nanosheets (Figure 2D).[46−48] By carefully controlling the concentration and diffusion rates of the metal ion and organic linker solutions, 2D nanosheets are formed due to the diffusion of each layer. A representative example of diffusion-mediated modulation is CuBDC synthesis.[46] CuBDC is typically synthesized with this method, containing three different liquid layers. Synthesized CuBDC nanosheets were incorporated into various polymers such as Matrimid, PIM-1, and OPDA-TMPDA for excellent CO_2/CH_4 separation. This method can produce nanosheets with uniform thickness and composition, but the reaction conditions, such as concentrations, temperature, and pH, should be precisely adjusted.

The seed growth method involves the controlled nucleation and growth of MOF and zeolite nanosheets on predefined seed crystals or substrates (Figure 2E).[39,49] Jeon et al. first reported the bottom-up synthesis of MFI nanosheets without the formation of orthogonal intergrowths.[49] By the hydrothermal seed growth method, MFI nanocrystal seeds were first grown cylindrical, and faceted nanosheets appeared from the corner. While the nanosheets grow, they encircle the original seed with uniform thickness and well-defined facets with preferred b orientation. This method can produce well-ordered, high-aspect-ratio 2D nanosheets with a high degree of control over their shape and size. However, it has a high level of difficulty, and only a few zeolite materials have been reported with this method.

Utilizing a substrate with suitable crystallographic orientation, substrate-assisted growth directs the alignment of MOF or zeolite nanosheets during synthesis (Figure 2F).[50−52] Stassen et al. demonstrated a CVD process for ZIF-8 film formation.[50] Homogeneous ZIF-8 thin films with uniform thickness were fabricated by depositing the metal oxide first. A consecutive vapor reaction step is followed for oxide-to-MOF transformations. However, by the substrate-assisted growth method, it is impossible to obtain the product in powder form, which restricts further applications. To use them in gas separation membranes, additional treatment, such as polymer impregnation, is needed.

Ideally, a 2D material has a thickness at the atomic level. In the case of zeolites and MOFs, it is accurate to define 2D materials as having a thickness on the order of a few unit cells. However, since the aspect ratio is more critical than the thickness for enhancing separation performance, nanoplates with high aspect ratios can also be utilized in membrane fabrication. Conversion methods are known to make relatively thick nanoplates. The conversion method is typically used in MOF synthesis rather than for zeolites. Since MOFs are combinations of metal nodes and organic linkers, metal precursors are used for conversion by postligand treatment. The two most typical precursor types are metal oxide and metal hydroxide (Figure 2G,H). In the case of metal oxide conversion, zinc oxide sphere and nanorod templates were used for conversion to ZIF-8.[53−55] For most metal oxide conversion cases, precursors are partially converted only at the surface. Precursors remained in the synthesized particles, which is improper for gas separation since unconverted areas in the metal oxide can serve as a barrier layer, significantly reducing separation performance. Moreover, a nonplanar shape template morphology is improper for high-aspect-ratio control. Meanwhile, a high-aspect-ratio zinc layered hydroxide template successfully led to perfect conversion to ZIF-8 maintaining a high aspect ratio. ZIF-8 nanoplates reported by Kim's group showed perfect conversion without precursor remaining.[14,56] With the addition of ZIF-8 nanoplates into the PI membrane, superior C_3H_6/C_3H_8 and H_2/C_3H_8 separation performances of the MMM compared with isotropic particles were reported.

Furthermore, the growth of MOF and zeolite nanoparticles on the surfaces of two-dimensional counterparts like graphene has been reported.[57,58] Generally, oxidized graphene offers favorable sites for interacting with MOF and zeolite precursors due to its surface oxygen functional groups, resulting in high particle densities on the graphene surface. However, due to graphene's gas barrier properties, the enhancement in gas performance is limited, and despite potential additional pores,
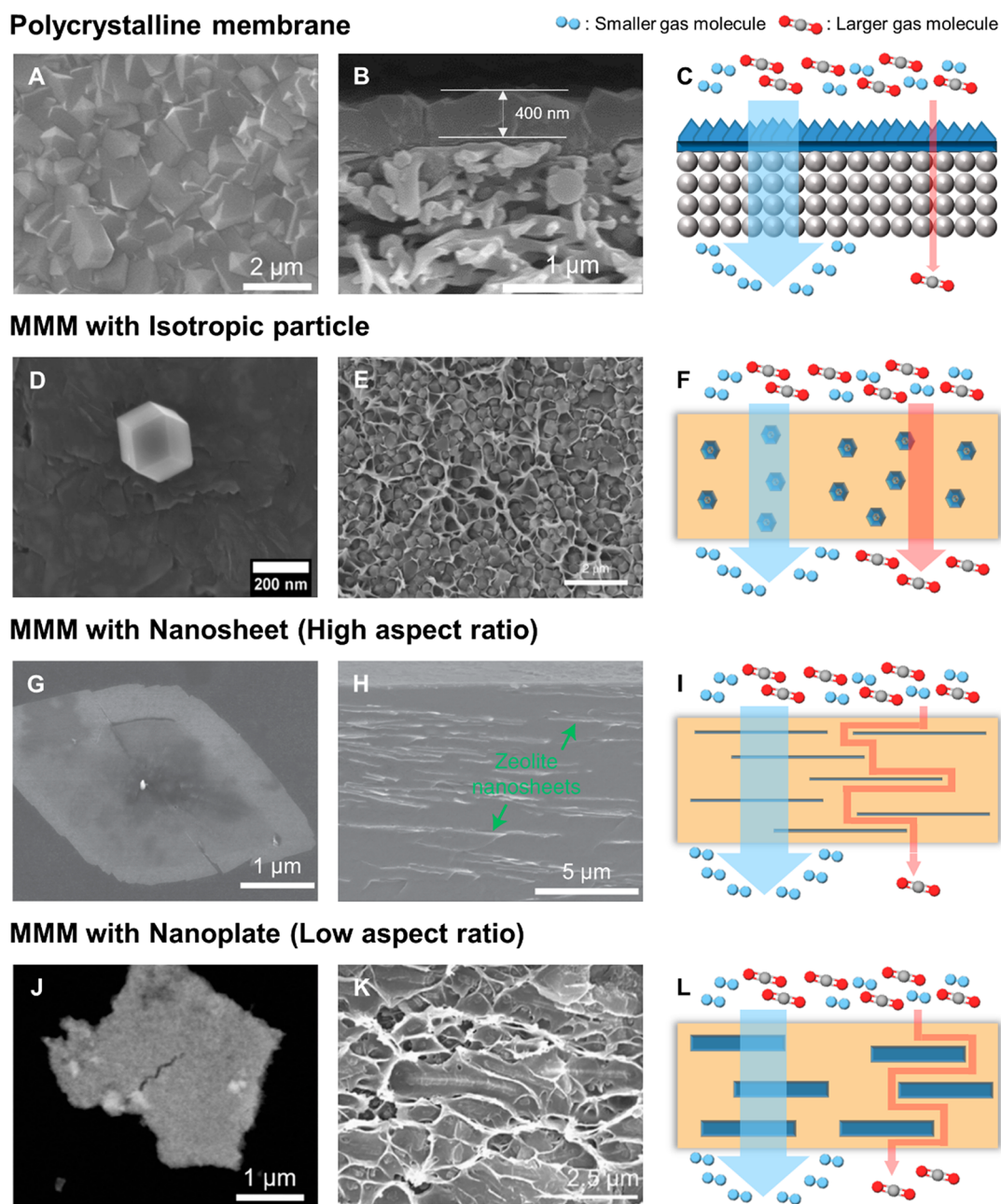
Figure 3. Structure and gas permeation mechanism of membranes with different filler morphology. (A−C) Polycrystalline membrane: Top and cross-sectional SEM images of ZIF-8 membrane and its gas permeation mechanism. Reproduced with permission from ref 59. Copyright 2021 Wiley-VCH. (D−F) MMM with isotropic particles: (D) SEM image of an isotropic ZIF-67 particle; (E) cross-sectional SEM image of 43 wt % ZIF-67/6FDA-DHTM-durene MMM; (F) gas permeation mechanism. Reproduced with permission from ref 60. Copyright 2020 the authors of ref 60, under exclusive license to Springer Nature. (G−I) MMM with high-aspect-ratio nanosheet: (G) SEM image of MFI nanosheet; (H) cross-sectional SEM image of 3 wt % MFI/Nafion MMM; (I) gas permeation mechanism. Reproduced with permission from ref 61. Copyright 2022 the authors of ref 61, under exclusive license to Springer Nature. (J−L) MMM with low-aspect-ratio nanoplate: (J) SEM image of ZIF-8 nanoplate; (K) cross-sectional SEM image of 20 wt % ZIF-8 nanoplate/6FDA-DAM; (L) gas permeation mechanism. Reproduced with permission from ref 14 (copyright 2023 Elsevier) and from ref 56 (CC BY-NC 4.0).

the graphene's pore density remains relatively low, resulting in less effective enhancement of separator performance compared to single-crystal nanosheets. Nonetheless, this approach offers the advantage of facile preparation of diverse structures by selecting appropriate precursors, while the aspect ratio can be readily tuned based on graphene's dimensions.

PROPERTIES OF MMMS WITH DIFFERENT FILLER MORPHOLOGIES

MOFs and zeolites can be directly synthesized into membranes on porous supports using solvothermal approaches, in situ growth, vapor conversion, and electrochemical deposition.[62] Commonly employed porous supports include materials like alumina or silica, occasionally supplemented with gutter layers to enhance mechanical stability, tune pore rigidity, and enable the deposition of thin selective layers.[59,63,64] These polycrystal-

line membranes exhibit remarkable separation efficiency, due to their intrinsic structural characteristics that yield well-defined and interconnected pore networks. However, preparing continuous films over substantial areas, free from grain boundary defects and inter/intracrystalline fissures, remains challenging, as these imperfections serve as nonselective pathways, compromising separation efficacy. Notably, these membranes are comparatively facile to fabricate at thin thicknesses, typically on the submicrometer scale. Figure 3A,B shows an example of a ZIF-8 polycrystalline membrane. A 400 nm thick ZIF-8 membrane was fabricated on a PES polymer support with a graphene oxide nanoribbon gutter layer.[59] Using a selective MOF or zeolite layer, gas molecules readily traverse the membrane while relatively larger molecules encounter effective obstruction, resulting in markedly enhanced selectivity (Figure 3C).

Despite their exceptional performance, polycrystalline membranes are prone to brittleness and are predominantly synthesized via hydrothermal reactions, limiting broader industrial applications. Particularly in the case of zeolite membranes, additional post-thermal treatment is required to remove organic SDAs, further complicating the creation of large-scale membranes with exceptionally thin selective layers. While separators utilizing polycrystalline coatings find application in separation processes, they also serve a significant role in elucidating the gas permeation characteristics of crystalline materials. The amalgamation of gas permeation data acquired from polymers and that extracted from polycrystalline separators facilitates the predictive determination of efficient composite pairings, circumventing the need for direct experimental validation. Notably, as the effectiveness of MMMs is substantially governed by the properties of the filler component, a profound comprehension of the separation efficacy intrinsic to the filler becomes imperative for the advancement of high-performance membranes.

Beyond the inherent pore structure of filler materials, the gas separation mechanism in MMMs can notably diverge based on the shape of the filler. Consequently, we have categorized MMMs into three distinct groups: those incorporating isotropic particles, those featuring high-aspect-ratio fillers (nanosheets), and those containing low-aspect-ratio fillers (nanoplates). MMMs involving isotropic particles have been extensively investigated across various literature due to their straightforward synthesis procedure. These particles are generally synthesized at a scale of hundreds of nanometers or smaller and subsequently integrated into a polymer solution, which is cast to form the membrane. Figure 3D shows an isotropic ZIF-67 particle with a size of 200 nm.[60] Then, ZIF-67 particles were hybridized with 6FDA-DHTM-Durene polymer for C_3H_6/C_3H_8 separation (Figure 3E). Their introduction into the membrane can induce alterations in chain mobility and packing within the polymer matrix. By creating additional fractional free volume, these particles facilitate the movement of permeating molecules. Importantly, molecular sieving predominantly occurs through the apertures of these particles, leading to accelerated permeation of smaller molecules. Consequently, MMMs incorporating isotropic particles typically exhibit a moderate enhancement in both permeability and selectivity (Figure 3F). However, due to the tendency of fillers to aggregate, the filler content is commonly limited to below 30 wt % to avert the creation of nonselective paths.[15,65] This limitation results in performance of MMMs with isotropic particles falling short of

the intrinsic capabilities of the fillers yet surpassing that of pure polymer membranes.

Incorporating high-aspect-ratio nanosheet fillers offers the potential for further enhancement of separation performance while retaining the advantages associated with isotropic particles. Nanosheets are typically synthesized or prepared at a scale of a few nanometers thickness with a pronounced aspect ratio, as evidenced by the SEM images of MFI nanosheets in Figure 3G.[61] The high-aspect-ratio structure provides a substantial surface-to-volume ratio and allows high filler loading when fabricating membranes (Figure 3H) because nanosheets prefer to be aligned in the confined spacing.[61,65] In cases where nanosheets are well-aligned, they introduce intricate pathways that impede the passage of larger molecules exceeding the aperture size, thereby reducing the permeability (Figure 3I). Simultaneously, the nanosheets permit the penetration of smaller molecules through their pores, resulting in maximized selectivity.

Remarkably, nanosheets are anticipated to enhance membrane separation performance even with a minor addition of filler. This attribute holds significance in practical applications, as it avoids altering polymer properties due to filler incorporation and helps reduce material costs. Nonetheless, the synthesis process is commonly laborious with low yield.[66] Moreover, it is still questionable whether the separation performance of bulk crystals can be retained in nanosheets with just a few unit-cell thicknesses. The prevalence of external pores in these nanosheets might potentially result in pore blocking by infiltrating polymer chains, raising questions about their functionality.

Nanoplates, characterized by a relatively modest aspect ratio, present an alternate filler material for preparing MMMs, offering benefits akin to those of nanosheets. Unlike nanosheets, which manifest as single-crystalline structures with a solitary orientation, nanoplates adopt polycrystalline configurations comprising densely assembled particles.[56] Nanosheets are typically obtained via direct synthesis or exfoliation from layered bulk materials, accounting for their single-crystal attributes. In contrast, nanoplates are commonly derived through the conversion of precursor nanosheets or the growth of densely packed nanoparticles on substrates like graphene oxide or other 2D materials.[14,56,57] Consequently, nanoplates exhibit marginally increased thicknesses alongside lower aspect ratios, as exemplified by the ZIF-8 nanoplate prepared through the conversion approach (Figure 3J).[14,56]

The prepared MMM displays a cross-sectional arrangement wherein nanoplates are enveloped by polymer chains without interfacial voids (Figure 3K). The gas permeation mechanism of the MMM with nanoplates is depicted in Figure 3L. Given that nanoplates possess a lower aspect ratio in comparison to nanosheets, the influence of tortuous pathways is relatively reduced, consequently yielding slightly reduced selectivity. However, nanoplates can resemble the nanosheet effects owing to their similar morphology, setting them apart from isotropic particles. Furthermore, when the orientation of nanoplates aligns vertically within the MMM, the structure can provide fast and selective gas permeation pathways due to its increased thickness, which is enough to provide a permeation channel for permeable molecules.[56]
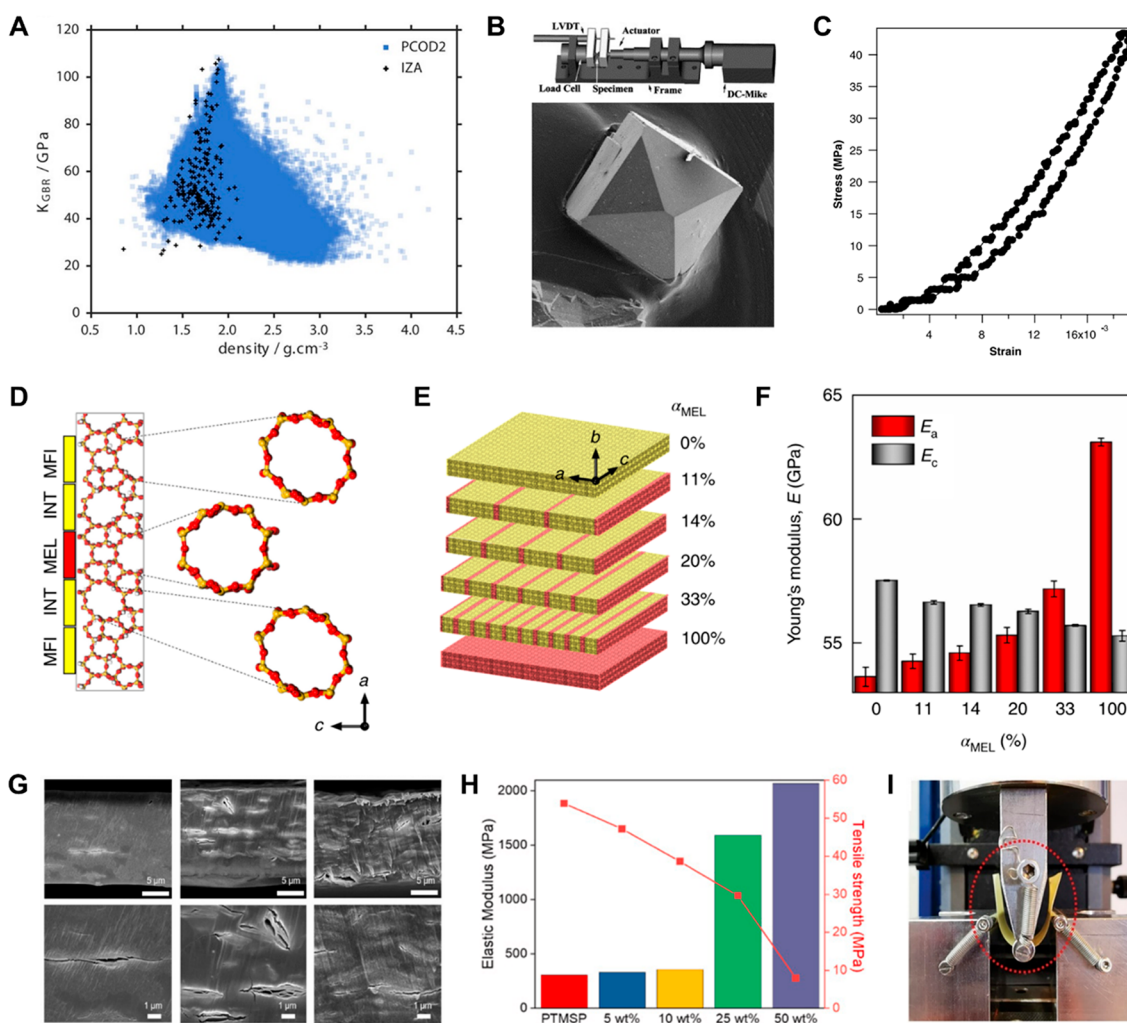
Figure 4. (A) Bulk modulus distributions of zeolites predicted using machine learning-assisted calculation. Reproduced from ref 67. Copyright 2017 American Chemical Society. (B) Microdeformation tester and single zeolite crystal and (C) mechanical test result. Reproduced with permission from ref 68. Copyright 2002 Elsevier. (D) Structure image of MEL-inserted MFI zeolite, (E) one-dimensional growth of MEL-inserted MFI zeolite nanosheet depending on the MEL content, and (F) calculated elastic modulus depending on MEL content. Reproduced with permission from ref 34. Copyright 2020 the authors of ref 34, under exclusive license to Springer Nature. (G) Cross-sectional SEM images of MMM with 2D nanosheet filler and (H) their mechanical stability test result. Reproduced with permission from ref 15. (I) Three-point bending test image showing the flexibility of high 2D-zeolite-loaded MMM. Reproduced with permission from ref 69. Copyright 2022 the authors of ref 69, under exclusive license to the American Association for the Advancement of Science.

MMMS WITH HIGH-ASPECT-RATIO NANOSHEETS (ZEOLITE-TYPE)

Considering the cases of graphene/polymer composites and nanoclay/polymer composites, it is well-known that 2D materials can enhance polymer mechanical properties due to several reasons, such as their high intrinsic strength and stiffness, large surface area for improved interactions, barrier effects on chain movement, reinforcement at the nanoscale, flexibility for better bonding, fracture toughness improvement, and reduced polymer chain mobility.[70−72] Therefore, it is rational to expect that zeolite or MOF nanosheets will also have similar effects on polymers, while the degree of enhancement must be lower than that with graphene due to the lower mechanical properties of zeolites and MOFs compared with graphene.[73,74] In addition, the enhancement is highly dependent on the properties of the polymer. For example, polyimide has much stronger mechanical properties than rubbery polymers, while both polymers can be used depending on the target gas pair.[75]

Figure 4 exemplifies the mechanical attributes of pure zeolites and zeolite fillers integrated within MMMs. Zeolite was selected because of its good mechanical properties compared with MOFs. In Figure 4A, the bulk modulus (K) of zeolites is portrayed, leveraging data from both the IZA framework database and the silica zeolite database (PCOD2). The density-related distribution of bulk modulus, as deduced through machine learning assistance from the zeolite database, is correlated with zeolite density.[67] Notably, higher-density zeolites exhibit lower bulk modulus values compared to their lower-density counterparts. However, an appreciable segment of estimated zeolite bulk moduli surpass 20 GPa, outperforming the values characteristic of most polymer matrices. In further support of zeolites' exceptional mechanical traits, empirical validation is furnished through microdeformation assessments (Figure 4B,C).[68] These examinations were conducted with ZSM-5 crystals (MFI-type zeolite, approximately 0.5 mm in size) subjected to mechanical testing. The stress−strain curve derived from microdeformation analysis is presented in Figure
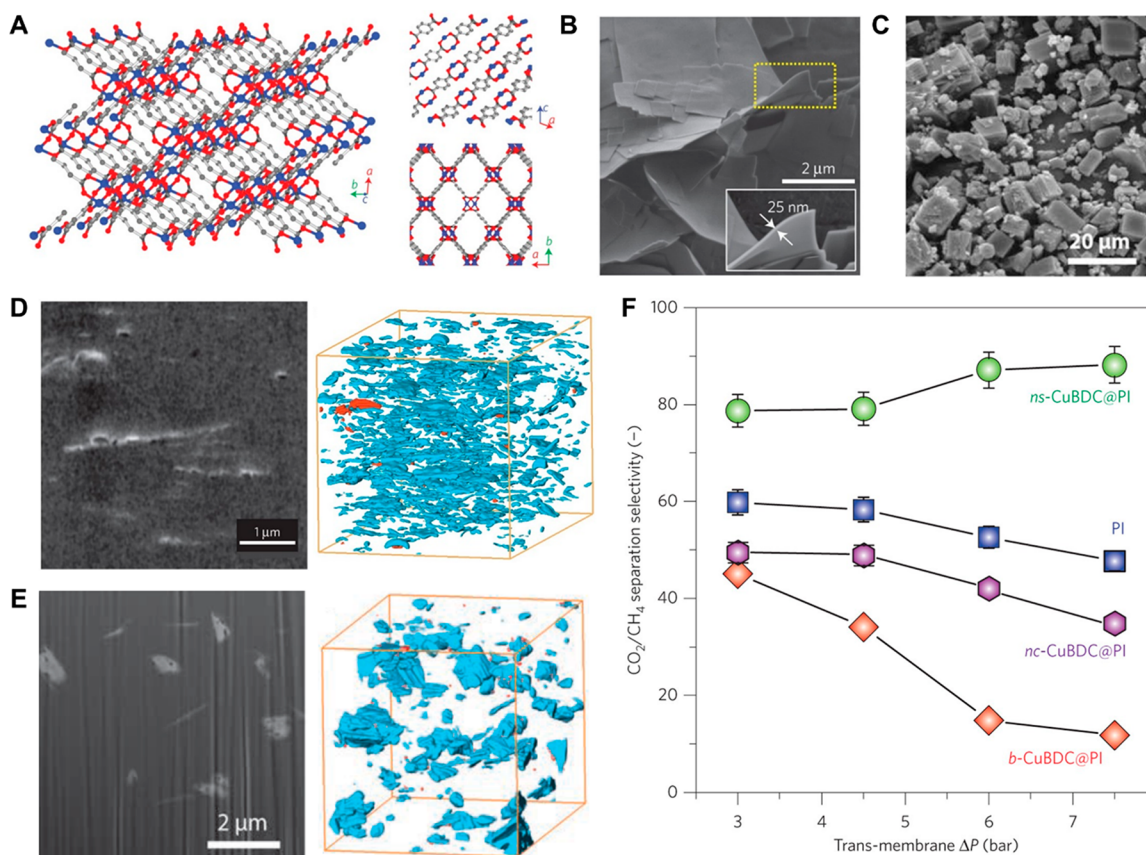
Figure 5. (A) Crystal structure of CuBDC with views along different crystallographic axes. (B, C) SEM images of (B) CuBDC nanosheet and (C) CuBDC nanocube. (D, E) Cross-sectional SEM images and surface-rendered views of FIB-SEM tomograms for 8 wt % (D) CuBDC nanosheet/polyimide and (E) CuBDC nanocube/polyimide. Reproduced from ref 46. Copyright 2014 Springer Nature.

4C, revealing a notably elevated elastic modulus of 4 GPa. While the mechanical properties of bulk-scale three-dimensional (3D) zeolites are found to extend to 2D zeolites, it is acknowledged that intergrowth of distinct zeolite types might instigate mechanical property variations. For instance, Tsapatsis's group prepared MFI nanosheets,[34] demonstrating that MEL-type zeolites can propagate unidirectionally upon the manufactured MFI zeolite nanosheets (Figure 4 D,E). Additionally, a computational simulation (Figure 4F) portrayed the one-dimensional advancement of zeolite MEL, potentially culminating in the reinforcement of the elastic modulus in a specific direction (*a* axis).

Leveraging zeolites with superior mechanical traits relative to polymer matrices underscores the alterations in mechanical characteristics within zeolite-filler MMMs. In the context of MMMs synthesized using PTMSP and MFI nanosheets (Figure 4G), cross-sectional SEM images affirm the successful creation of the MMM, with fillers in the polymer matrix maintaining orientation despite the substantial filler content.[15] Consequently, Figure 4H presents an enhancement in the mechanical properties of MMMs as measured by increasing zeolite content. Paradoxically, despite the augmented mechanical properties, the composite films with substantial zeolite concentrations also exhibit flexibility, even at elevated filler loads (Figure 4I). This observation is different from typical behavior observed in MMMs with isotropic fillers. Consequently, the utilization of high-aspect-ratio fillers appears more promising in achieving the dual objectives of enhancing durability and flexibility, which are critical factors for the industrial implementation of membranes.

MMMS WITH HIGH-ASPECT-RATIO NANOSHEETS (MOF-TYPE)

Rodenas et al. introduced a diffusion-mediated modulation synthesis strategy for dispersible CuBDC MOF lamellae, characterized by a layered crystalline structure conducive to the selective adsorption of polar gas molecules (Figure 5A).[46] This approach involves a liquid medium with three layers, enabling the controlled diffusion of Cu^{2+} cations and BDCA linker precursors to facilitate MOF growth in a localized, diluted environment. Synthesized CuBDC nanosheets (ns-CuBDC) displayed lateral dimensions of 0.5−4 μm and thicknesses spanning 5−25 nm, exhibiting an aspect ratio exceeding 20 (Figure 5B). In contrast, conventional solvothermal synthesis yielded isotropic cubic crystals (nc-CuBDC) (Figure 5C). Both types of fillers were integrated into a polyimide (PI) matrix for gas separation testing.

The internal structure of the resulting MMMs was scrutinized using tomographic focused ion beam scanning electron microscopy (FIB-SEM), generating 3D reconstructions (Figure 5D,E). Despite equal filler content, ns-CuBDC showed uniform dispersion throughout the polymer matrix, whereas nc-CuBDC left significant unoccupied polymer volume. In evaluating MMMs and PI membranes as a reference for CO_2 separation from CO_2/CH_4 mixtures, different MMMs were tested under varying pressure differences (Figure 5F). The incorporation of 8 wt % bulk-type CuBDC (b-CuBDC) and nc-CuBDC led to a slight selectivity reduction compared to the neat PI membrane, attributed to filler-induced disruption of polymer chains and subsequent nonselective void formation. Conversely, ns-
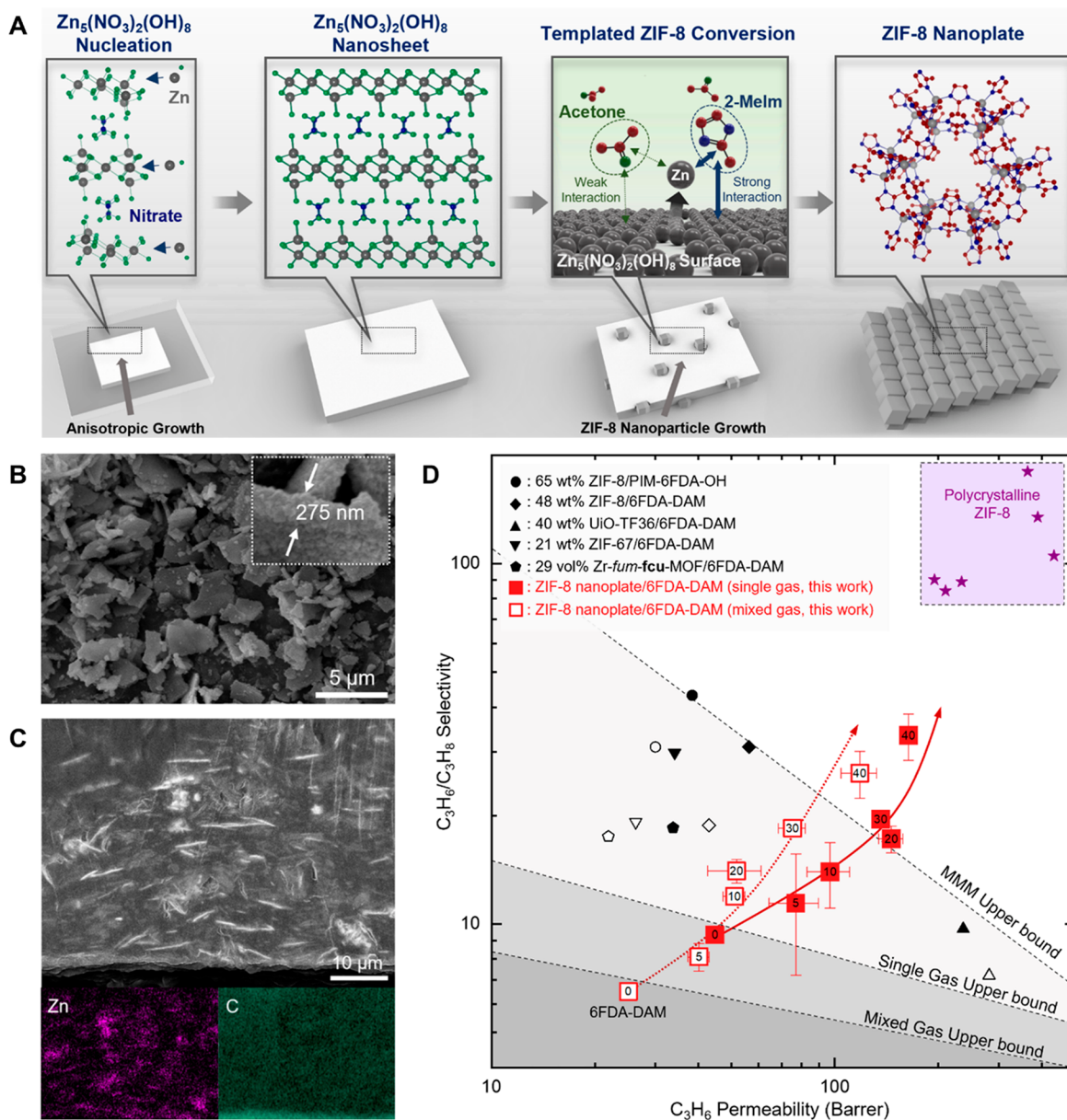
Figure 6. (A) Conversion process of $Zn_5(NO_3)_2OH_8$ nanosheet to ZIF-8 nanoplate. (B) SEM image of synthesized ZIF-8 nanoplates. (C) Cross-sectional SEM image of 40 wt % ZIF-8 nanoplate/6FDA-DAM and corresponding EDS mapping images of zinc and carbon. (D) C_3H_6/C_3H_8 separation performance of ZIF-8 nanoplate/6FDA-DAM membranes. From ref 56. CC BY-NC 4.0).

CuBDC integration demonstrated superior performance due to enhanced gas interaction resulting from its homogeneous distribution. Notably, the selectivity increased with elevated upstream pressure, demonstrating the potential of high-aspect-ratio nanosheet fillers to mitigate polymer matrix swelling. In summary, ultrathin high-aspect-ratio nanosheets decrease membrane thickness, ensuring well-dispersed fillers that enhance permeability, selectivity, and resistance to plasticization effects.

MMMS WITH LOW-ASPECT-RATIO NANOPLATES

While ZIF-8 is one of the most widely used MOFs for gas separation, synthesizing ZIF-8 nanosheets poses challenges due to factors such as controlling nucleation and growth kinetics, templating agents, crystal growth conditions, and scalability. Figure 6 presents an alternative approach to preparing ZIF-8 nanoplates with an aspect ratio of 20, evaluated for C_3H_6/C_3H_8

separation.[56] The ZIF-8 aperture size is 3.4 Å, which expands to approximately 4.0 Å due to organic linker flexibility. Unlike single-crystal nanosheets with planar surfaces aligned to specific crystallographic orientations and atomic-scale thickness, ZIF-8 nanoplates are polycrystalline and exhibit a relatively lower aspect ratio yet share structural benefits akin to nanosheets. Synthesis of ZIF-8 nanoplates employed a template-assisted conversion method (Figure 6A). $Zn_5(NO_3)_2OH_8$ nanosheets were utilized as metal templates, and the injection rate and appropriate solvent of 2-methylimidazole linkers were optimized to facilitate phase conversion while retaining a sheetlike morphology. The resultant ZIF-8 nanoplates displayed an average lateral size of 4 μm and thickness around 200 nm, yielding an aspect ratio of 20 (Figure 6B). To demonstrate the influence of the sheetlike morphology, ZIF-8 nanoplates were hybridized with the 6FDA-DAM polymer matrix. Employing the bar coating method with shear force achieved a highly aligned
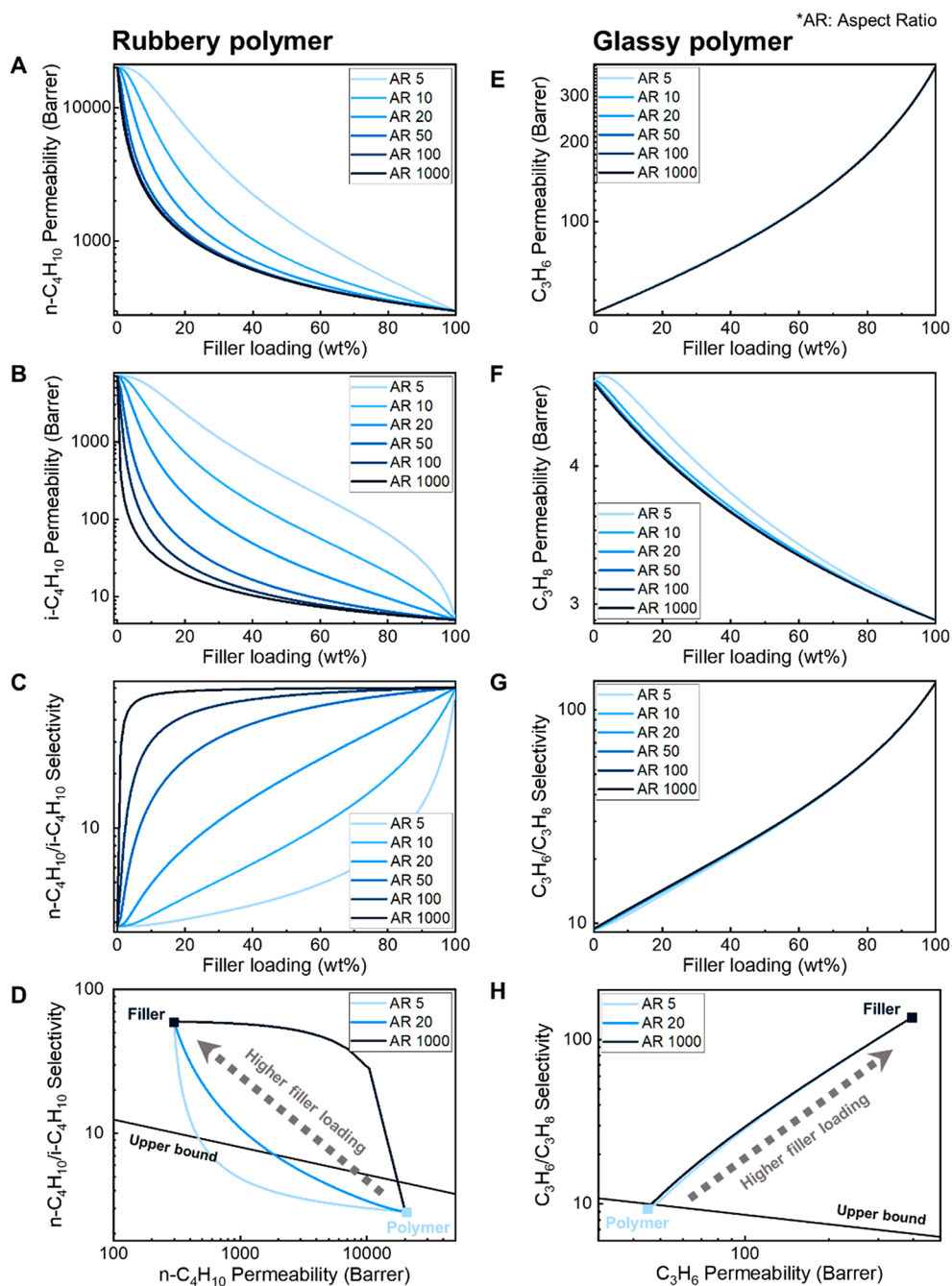
Figure 7. Prediction of separation performance calculated by the modified Cussler model. (A–D) Calculated results for MFI/PTMSP: (A) n-C_4H_{10} permeability, (B) i-C_4H_{10} permeability, (C) n-C_4H_{10}/i-C_4H_{10} selectivity, and (D) separation performance of MFI/PTMSP with different aspect ratios (ARs) of MFI zeolite. (E–H) Calculated results for ZIF-8/6FDA-DAM: (E) C_3H_6 permeability, (F) C_3H_8 permeability, (G) C_3H_6/C_3H_8 selectivity, and (H) separation performance of ZIF-8/6FDA-DAM with different ARs of ZIF-8 nanosheets.

filler distribution in membrane fabrication. Remarkably, ZIF-8 nanoplates were uniformly dispersed and aligned within the polymer matrix, even at a substantial 40 wt % loading (Figure 6C). EDS mapping unveiled a predominant horizontal alignment of ZIF-8 nanoplates, evident through even carbon species detection, while Zn species were confined to the nanoplate locations. C_3H_6/C_3H_8 separation performance was gauged across MMMs with varying filler loading under both single-gas and mixed-gas conditions (Figure 6D). In both scenarios, performance escalated with increased filler loading, surpassing upper bounds. In single-gas separation testing, the C_3H_6 permeability registered 164 barrer with a C_3H_6/C_3H_8 selectivity

of 33.4, and for mixed-gas separation, the C_3H_6 permeability was measured as 118.2 Barrer with a C_3H_6/C_3H_8 selectivity of 26.2. These accomplishments outperformed isotropic-particle-based MMMs, indicating the importance of the filler shape because their sieving properties can be maximized, as C_3H_6 molecules permeate the crystals while C_3H_8 molecules are impeded due to heightened in-plane tortuosity.

In addition, the composite membranes were tested for hydrogen extraction with mechanical properties comparison.[14] A 20 wt % ZIF-8 nanoplate/PI membrane exhibited high mechanical properties of 0.282 GPa for hardness and 3.5 GPa for modulus, which are higher than those of ZIF-8 isotropic/PI

membranes. Furthermore, high-aspect-ratio fillers allowed significant enhancement in hydrogen separation performance, showing a hydrogen permeability of around 1800 barrer with a hydrogen/propane selectivity of 260 at 20 wt % ZIF-8 nanoplate loading, which is much enhanced relative to the membrane with isotropic ZIF-8 particles.

PREDICTION OF SEPARATION PERFORMANCE WITH POLYMER TYPES AND NANOSHEET ASPECT RATIO

Fabricating 2D materials with precisely controlled aspect ratios is still challenging. However, it is possible to predict separation performance with mathematical models to guide future research.[76,77] The modified Cussler model was introduced to predict permeability and selectivity among various mathematical models that predict separation performances of polymeric membranes mixed with fillers.[78] The modified Cussler model is a mathematical model considering diffusion through a well-aligned array of two-dimensional fillers in the polymer matrix. The calculation model predicts the permeability using the following equation:

$$P_i^C = \frac{P_i^M}{(1 - \phi) + \frac{1}{\left[\left(\frac{1}{\phi}\right)\left(\frac{P_i^F}{P_i^M}\right) + \left(\frac{(1 - \phi)}{\alpha^2 \phi^2}\right)\right]}}$$

where α is the aspect ratio of the filler, ϕ is the volume fraction of the filler, P_i^C is the permeability of gas i through the mixed-matrix membrane, P_i^M is the permeability of gas i through the pure polymer matrix, and P_i^F is the permeability of gas i through the filler.

The permeability and selectivity of MMMs incorporating fillers with different aspect ratios were evaluated for rubbery and glassy polymers. For rubbery-polymer-based MMMs targeting butane isomer separation, MFI-type zeolite and PTMSP were chosen. Calculations utilized single gas permeability values of 300 barrer for n-butane and 5 barrer for i-butane in MFI nanosheets, while PTMSP's single gas permeability values of 6200 barrer for n-butane and 1040 barrer for i-butane were experimentally determined.[37,79] Incorporating MFI nanosheets led to decreased permeability for both isomers due to higher tortuosity, which was especially pronounced with higher aspect ratios (Figures 7A,B). Notably, MFI acted as a barrier for i-butane while permitting n-butane passage through pores, though at a lower rate than the pristine polymer. Consequently, i-butane permeability reduction drove an increase in overall n-butane/i-butane selectivity with rising MFI content (Figure 7C). Remarkably, a high-aspect-ratio MFI at even modest loading approached the intrinsic selectivity of the filler. In contrast, low-aspect-ratio MFI, such as isotropic particles, required substantially higher loading to exceed the upper bound, as illustrated in Figure 7D. This demonstrates that high-aspect-ratio MFI achieves commercially attractive results with minimal filler, while low-aspect-ratio MFI necessitates elevated loading to attain comparable performance.

For glassy-polymer-based MMMs targeting propylene/ propane separation, ZIF-8 and 6FDA-DAM polyimide were chosen. Calculations utilized ZIF-8 single gas permeabilities of 390 barrer for propylene and 2.9 barrer for propane, while the 6FDA-DAM membrane's single gas permeability values were experimentally determined as 44.8 barrer for propylene and 4.8 barrer for propane.[56] Unlike the rubbery-polymer-based model, various aspect ratios in the glassy-polymer-based model showed minimal separation performance differences. The C_3H_6 permeability remained consistent even for aspect ratios between 5 and 1000 (Figure 7E). Slight variations in C_3H_8 permeability were attributed to increased tortuosity yet remained negligible (Figure 7F), as further evident in C_3H_6/C_3H_8 selectivity (Figure 7G). With increasing filler loading, both the permeability and selectivity displayed similar trends for high and low aspect ratios (Figure 7H), stemming from the inherently low permeability of glassy polymers. This results in similar calculated separation performances between the initial point (polymer) and the final point (filler). In glassy-polymer-based MMMs, high filler content proves more crucial than a high aspect ratio of the filler. However, high aspect ratio remains beneficial, enhancing filler dispersibility and compatibility within the polymer matrix and facilitating defect-free fabrication of highly loaded MMMs. This underscores that while a high aspect ratio may not dramatically impact glassy-polymer-based MMM separation, its influence on structural integrity and processability remains valuable. In particular, with the orientation control of the filler, the permeability of permeable gas molecules can be enhanced significantly, which can be referred from the case of binary-phase composite membranes or MMMs with phase separations.[61]

Of course, the model presumes flawless dispersion and alignment of fillers within the polymer matrix, with no vacant spaces between them. Hence, it necessitates validation against real experimental data. Several papers convey disparities in experimental results and theoretical predictions, mostly in permeability.[15,29,56] Shete et al.[29] indicated that for certain types of polymers, the model predictions were much lower than the experimental values. Also, Kwon, Kim, and co-workers[15,56] suggested that the reason for the difference is loosely aligned fillers. Nonselective voids by inadequate adhesion between filler and polymer can lead gases to bypass, which results in high permeability. These inconsistencies become more severe at elevated filler loadings due to filler aggregation. Choi et al.[15] showed an excellent match between the calculation and experimental data until 5 wt %, whereas great deviation appeared at a higher filler ratio. Nonetheless, our calculations provide insight into the design of the filler structure and composite materials in addition to the selection of the combination of filler materials and polymers.

CONCLUSIONS AND OUTLOOK

We have reviewed the recent research trend of MMMs for gas separation applications, focusing on the integration of high-aspect-ratio 2D MOFs and zeolites. Various methods for preparing 2D materials have been outlined, providing the application for the fabrication of composite membranes. Membrane types are categorized ranging from polycrystalline membranes to MMMs with different filler structures. This exploration has revealed that composite membranes with high-aspect-ratio fillers hold potential due to their ability to enhance molecular sieving and gas transport. Considering polymer types and nanosheet aspect ratios, composite membranes can provide a clear path for optimizing separation performance. While substantial progress has been made in understanding the synergetic effects of 2D materials and polymers, several opportunities and challenges remain. 2D MOFs and zeolites are rarely reported for gas separation applications. To fabricate high-functioning and high-loading MMMs, carefully choosing an appropriate combination of filler and polymer and ensuring compatibility and adhesion between these components are essential. To create high-performance composite membranes, a

large-area coating of a polymer and filler solution on a support with a submicrometer thickness is required, followed by modularization of the resulting membranes. Considering that continuous coating processes of other 2D materials such as graphene have been reported recently and that most MMMs are reported as thick free-standing films with reported permeability, a technology for forming ultrathin selective layers on a large area by a method such as slow die coating should be developed for practical applications.[24,80] Furthermore, it is required to evaluate membrane performance under harsh operating conditions. By addressing stability and durability concerns, it is possible to accelerate the adoption of 2D-material-based composite membranes for practical applications at the industry level. Insights gained from these studies could find relevance in diverse areas, including proton exchange membrane fuel cells, batteries, and water treatment, fostering innovation and sustainability across multiple fields.

■ AUTHOR INFORMATION

Corresponding Author

Dae Woo Kim − *Department of Chemical and Biomolecular Engineering, Yonsei University, Seoul 03722, Republic of Korea*; ⊙ orcid.org/0000-0001-6533-8086; Email: audw1105@yonsei.ac.kr

Authors

Minsu Kim − *Department of Chemical and Biomolecular Engineering, Yonsei University, Seoul 03722, Republic of Korea*; ⊙ orcid.org/0000-0001-6277-2039
Wooyoung Choi − *Department of Chemical and Biomolecular Engineering, Yonsei University, Seoul 03722, Republic of Korea*
Choong Hoo Lee − *Department of Chemical and Biomolecular Engineering, Yonsei University, Seoul 03722, Republic of Korea*

Complete contact information is available at:
https://pubs.acs.org/10.1021/acsmaterialsau.3c00072

Author Contributions

CRediT: M.K. conceptualization (supporting), visualization (lead), writing—original draft (lead); W.C. conceptualization (supporting), writing—original draft (supporting); C.H.L. data curation (supporting); D.W.K. conceptualization (lead), funding acquisition (lead), supervision (lead), writing—original draft (lead) CRediT: **Minsu Kim** conceptualization, visualization, writing-original draft, writing-review & editing; **Wooyoung Choi** conceptualization, writing-original draft; **Choong Hoo Lee** data curation; **Dae Woo Kim** conceptualization, funding acquisition, supervision, writing-original draft, writing-review & editing.

Notes

The authors declare no competing financial interest.

■ ACKNOWLEDGMENTS

■ REFERENCES

(1) Park, H. B.; Kamcev, J.; Robeson, L. M.; Elimelech, M.; Freeman, B. D. Maximizing the right stuff: The trade-off between membrane permeability and selectivity. *Science* **2017**, *356* (6343), No. eaab0530.
(2) Baker, R. W.; Low, B. T. Gas separation membrane materials: a perspective. *Macromolecules* **2014**, *47* (20), 6999−7013.
(3) Kosinov, N.; Gascon, J.; Kapteijn, F.; Hensen, E. J. Recent developments in zeolite membranes for gas separation. *J. Membr. Sci.* **2016**, *499*, 65−79.
(4) Koros, W. J.; Fleming, G. Membrane-based gas separation. *J. Membr. Sci.* **1993**, *83* (1), 1−80.
(5) Wang, H.; Wang, M.; Liang, X.; Yuan, J.; Yang, H.; Wang, S.; Ren, Y.; Wu, H.; Pan, F.; Jiang, Z. Organic molecular sieve membranes for chemical separations. *Chem. Soc. Rev.* **2021**, *50* (9), 5468−5516.
(6) Robeson, L. M. The upper bound revisited. *J. Membr. Sci.* **2008**, *320* (1−2), 390−400.
(7) Hua, Y.; Park, S.; Choi, G. M.; Jung, H. J.; Cho, K. Y.; Jeong, H.-K. Highly propylene-selective asymmetric mixed-matrix membranes by polymer phase-inversion in sync with in-situ ZIF-8 formation. *Chem. Eng. J.* **2023**, *466*, 143048.
(8) Song, S.; Jiang, H.; Wu, H.; Zhao, M.; Guo, Z.; Li, B.; Ren, Y.; Wang, Y.; Ye, C.; Guiver, M. D.; et al. Weakly pressure-dependent molecular sieving of propylene/propane mixtures through mixed matrix membrane with ZIF-8 direct-through channels. *J. Membr. Sci.* **2022**, *648*, 120366.
(9) Dechnik, J.; Gascon, J.; Doonan, C. J.; Janiak, C.; Sumby, C. J. Mixed-matrix membranes. *Angew. Chem., Int. Ed.* **2017**, *56* (32), 9292−9310.
(10) Cheng, Y.; Ying, Y.; Japip, S.; Jiang, S. D.; Chung, T. S.; Zhang, S.; Zhao, D. Advanced porous materials in mixed matrix membranes. *Adv. Mater.* **2018**, *30* (47), 1802401.
(11) Goh, S. H.; Lau, H. S.; Yong, W. F. Metal-Organic Frameworks (MOFs)-Based Mixed Matrix Membranes (MMMs) for Gas Separation: A Review on Advance Materials in Harsh Environmental Applications. *Small* **2022**, *18* (20), 2107536.
(12) Eum, K.; Yang, S.; Min, B.; Ma, C.; Drese, J. H.; Tamhankar, Y.; Nair, S. All-nanoporous hybrid membranes: incorporating zeolite nanoparticles and nanosheets with zeolitic imidazolate framework matrices. *ACS Appl. Mater. Interfaces* **2020**, *12* (24), 27368−27377.
(13) Li, X.; Hou, J.; Guo, R.; Wang, Z.; Zhang, J. Constructing unique cross-sectional structured mixed matrix membranes by incorporating ultrathin microporous nanosheets for efficient CO_2 separation. *ACS Appl. Mater. Interfaces* **2019**, *11* (27), 24618−24626.
(14) Kim, M.; Yoo, S.; Kwon, O.; Choi, E.; Choi, W.; Ji, H.; Won, J. C.; Kim, Y. H.; Kim, D. W. ZIF-8 nanoplate/6FDA-DAM membrane for hydrogen extraction from propane dehydrogenation process. *J. Membr. Sci.* **2023**, *685*, 121952.
(15) Choi, W.; Park, J.-h.; Choi, E.; Kim, M.; Ji, H.; Kwon, O.; Kim, D.; Kim, D. W. Hybridizing zeolite MFI nanosheets with PTMSP membranes for enhanced butane isomer separations. *J. Membr. Sci.* **2023**, *677*, 121659.
(16) Liu, Y.; Sim, J.; Hailemariam, R. H.; Lee, J.; Rho, H.; Park, K.-D.; Kim, D. W.; Woo, Y. C. Status and future trends of hollow fiber biogas separation membrane fabrication and modification techniques. *Chemosphere* **2022**, *303*, 134959.
(17) Sun, X.; Sun, H.; Li, H.; Peng, H. Developing polymer composite materials: carbon nanotubes or graphene? *Adv. Mater.* **2013**, *25* (37), 5153−5176.
(18) Dong, G.; Hou, J.; Wang, J.; Zhang, Y.; Chen, V.; Liu, J. Enhanced CO_2/N_2 separation by porous reduced graphene oxide/Pebax mixed matrix membranes. *J. Membr. Sci.* **2016**, *520*, 860−868.
(19) Li, W.; Samarasinghe, S. A. S. C.; Bae, T.-H. Enhancing CO_2/CH_4 separation performance and mechanical strength of mixed-matrix

membrane via combined use of graphene oxide and ZIF-8. *J. Ind. Eng. Chem.* **2018**, *67*, 156−163.

(20) Ashirov, T.; Yazaydin, A. O.; Coskun, A. Tuning the transport properties of gases in porous graphene membranes with controlled pore size and thickness. *Adv. Mater.* **2022**, *34* (5), 2106785.

(21) O'Hern, S. C.; Jang, D.; Bose, S.; Idrobo, J.-C.; Song, Y.; Laoui, T.; Kong, J.; Karnik, R. Nanofiltration across defect-sealed nanoporous monolayer graphene. *Nano Lett.* **2015**, *15* (5), 3254−3260.

(22) Yuan, Z.; He, G.; Faucher, S.; Kuehne, M.; Li, S. X.; Blankschtein, D.; Strano, M. S. Direct chemical vapor deposition synthesis of porous single-layer graphene membranes with high gas permeances and selectivities. *Adv. Mater.* **2021**, *33* (44), 2104308.

(23) Kang, J.; Ko, Y.; Kim, J. P.; Kim, J. Y.; Kim, J.; Kwon, O.; Kim, K. C.; Kim, D. W. Microwave-assisted design of nanoporous graphene membrane for ultrafast and switchable organic solvent nanofiltration. *Nat. Commun.* **2023**, *14* (1), 901.

(24) Kim, J.; Kang, J.; Kim, J. P.; Kim, J. Y.; Kim, J. H.; Kwon, O.; Kim, D. W. Scalable fabrication of nanoporous multilayer graphene oxide membrane for organic solvent nanofiltration. *Carbon* **2023**, *207*, 162−171.

(25) Moghadam, P. Z.; Li, A.; Wiggin, S. B.; Tao, A.; Maloney, A. G.; Wood, P. A.; Ward, S. C.; Fairen-Jimenez, D. Development of a Cambridge Structural Database subset: a collection of metal-organic frameworks for past, present, and future. *Chem. Mater.* **2017**, *29* (7), 2618−2625.

(26) Chaikittisilp, W.; Okubo, T. No more trial and error for zeolites. *Science* **2021**, *374* (6565), 257−258.

(27) Wang, X.; Chi, C.; Zhang, K.; Qian, Y.; Gupta, K. M.; Kang, Z.; Jiang, J.; Zhao, D. Reversed thermo-switchable molecular sieving membranes composed of two-dimensional metal-organic nanosheets for gas separation. *Nat. Commun.* **2017**, *8* (1), 14460.

(28) Feng, S.; Bu, M.; Pang, J.; Fan, W.; Fan, L.; Zhao, H.; Yang, G.; Guo, H.; Kong, G.; Sun, H.; et al. Hydrothermal stable ZIF-67 nanosheets via morphology regulation strategy to construct mixed-matrix membrane for gas separation. *J. Membr. Sci.* **2020**, *593*, 117404.

(29) Shete, M.; Kumar, P.; Bachman, J. E.; Ma, X.; Smith, Z. P.; Xu, W.; Mkhoyan, K. A.; Long, J. R.; Tsapatsis, M. On the direct synthesis of Cu (BDC) MOF nanosheets and their performance in mixed matrix membranes. *J. Membr. Sci.* **2018**, *549*, 312−320.

(30) Roth, W. J. MCM-22 zeolite family and the delaminated zeolite MCM-56 obtained in one-step synthesis. *Stud. Surf. Sci. Catal.* **2005**, *158*, 19−26.

(31) Fan, W.; Wu, P.; Namba, S.; Tatsumi, T. A Titanosilicate That Is Structurally Analogous to an MWW-Type Lamellar Precursor. *Angew. Chem., Int. Ed.* **2004**, *43* (2), 236−240.

(32) Ji, H.; Choi, Y.; Choi, W.; Choi, E.; Kim, M.; Kim, J. Y.; Kwon, O.; Ji, Y.; Kim, D. W. Selective gas permeation through polymer-hybridized graphene oxide nanoribbon nanochannels: Towards enhanced H_2/CO_2 selectivity. *J. Membr. Sci.* **2023**, *683*, 121856.

(33) Choi, W.; Choi, S. E.; Seol, J. S.; Kim, J. P.; Kim, M.; Ji, H.; Kwon, O.; Kim, H.; Kim, K. C.; Kim, D. W. Polyethylene oxide-intercalated nanoporous graphene membranes for ultrafast H_2/CO_2 separation: Role of graphene confinement effect on gas molecule binding. *J. Membr. Sci.* **2022**, *660*, 120821.

(34) Kumar, P.; Kim, D. W.; Rangnekar, N.; Xu, H.; Fetisov, E. O.; Ghosh, S.; Zhang, H.; Xiao, Q.; Shete, M.; Siepmann, J. I.; et al. One-dimensional intergrowths in two-dimensional zeolite nanosheets and their effect on ultra-selective transport. *Nat. Mater.* **2020**, *19* (4), 443−449.

(35) Corma, A.; Diaz, U.; Domine, M. E.; Fornés, V. AlITQ-6 and TiITQ-6: Synthesis, Characterization, and Catalytic Activity. *Angew. Chem., Int. Ed.* **2000**, *39* (8), 1499−1501.

(36) Corma, A.; Fornes, V.; Diaz, U. ITQ-18 a new delaminated stable zeolite. *Chem. Commun.* **2001**, No. 24, 2642−2643.

(37) Zhang, H.; Xiao, Q.; Guo, X.; Li, N.; Kumar, P.; Rangnekar, N.; Jeon, M. Y.; Al-Thabaiti, S.; Narasimharao, K.; Basahel, S. N.; et al. Open-pore two-dimensional MFI zeolite nanosheets for the fabrication of hydrocarbon-isomer-selective membranes on porous polymer supports. *Angew. Chem., Int. Ed.* **2016**, *55* (25), 7184−7187.

(38) Choi, M.; Na, K.; Kim, J.; Sakamoto, Y.; Terasaki, O.; Ryoo, R. Stable single-unit-cell nanosheets of zeolite MFI as active and long-lived catalysts. *Nature* **2009**, *461* (7261), 246−249.

(39) Kim, D.; Ghosh, S.; Akter, N.; Kraetz, A.; Duan, X.; Gwak, G.; Rangnekar, N.; Johnson, J.; Narasimharao, K.; Malik, M. A.; et al. Twin-free, directly synthesized MFI nanosheets with improved thickness uniformity and their use in membrane fabrication. *Sci. Adv.* **2022**, *8* (14), No. eabm8162.

(40) Peng, Y.; Li, Y.; Ban, Y.; Jin, H.; Jiao, W.; Liu, X.; Yang, W. Metal-organic framework nanosheets as building blocks for molecular sieving membranes. *Science* **2014**, *346* (6215), 1356−1359.

(41) Peng, Y.; Li, Y.; Ban, Y.; Yang, W. Two-dimensional metal-organic framework nanosheets for membrane-based gas separation. *Angew. Chem.* **2017**, *129* (33), 9889−9893.

(42) Ding, Y.; Chen, Y.-P.; Zhang, X.; Chen, L.; Dong, Z.; Jiang, H.-L.; Xu, H.; Zhou, H.-C. Controlled intercalation and chemical exfoliation of layered metal-organic frameworks using a chemically labile intercalating agent. *J. Am. Chem. Soc.* **2017**, *139* (27), 9136−9139.

(43) Sabnis, S.; Tanna, V. A.; Gulbinski, J.; Zhu, J.; Nonnenmann, S. S.; Sheng, G.; Lai, Z.; Winter, H. H.; Fan, W. Exfoliation of surfactant swollen layered MWW zeolites into two-dimensional zeolite nanosheets using telechelic liquid polybutadiene. *Microporous Mesoporous Mater.* **2021**, *315*, 110883.

(44) Varoon, K.; Zhang, X.; Elyassi, B.; Brewer, D. D.; Gettel, M.; Kumar, S.; Lee, J. A.; Maheshwari, S.; Mittal, A.; Sung, C.-Y.; et al. Dispersible exfoliated zeolite nanosheets and their application as a selective membrane. *Science* **2011**, *334* (6052), 72−75.

(45) Liu, Y.; Qiang, W.; Ji, T.; Zhang, M.; Li, M.; Lu, J.; Liu, Y. Uniform hierarchical MFI nanosheets prepared via anisotropic etching for solution-based sub-100-nm-thick oriented MFI layer fabrication. *Sci. Adv.* **2020**, *6* (7), No. eaay5993.

(46) Rodenas, T.; Luz, I.; Prieto, G.; Seoane, B.; Miro, H.; Corma, A.; Kapteijn, F.; Llabrés i Xamena, F. X.; Gascon, J. Metal-organic framework nanosheets in polymer composite materials for gas separation. *Nat. Mater.* **2015**, *14* (1), 48−55.

(47) Yang, Y.; Goh, K.; Wang, R.; Bae, T.-H. High-performance nanocomposite membranes realized by efficient molecular sieving with CuBDC nanosheets. *Chem. Commun.* **2017**, *53* (30), 4254−4257.

(48) Samarasinghe, S.; Chuah, C. Y.; Yang, Y.; Bae, T.-H. Tailoring CO2/CH4 separation properties of mixed-matrix membranes via combined use of two-and three-dimensional metal-organic frameworks. *J. Membr. Sci.* **2018**, *557*, 30−37.

(49) Jeon, M. Y.; Kim, D.; Kumar, P.; Lee, P. S.; Rangnekar, N.; Bai, P.; Shete, M.; Elyassi, B.; Lee, H. S.; Narasimharao, K.; et al. Ultra-selective high-flux membranes from directly synthesized zeolite nanosheets. *Nature* **2017**, *543* (7647), 690−694.

(50) Stassen, I.; Styles, M.; Grenci, G.; Gorp, H. V.; Vanderlinden, W.; Feyter, S. D.; Falcaro, P.; Vos, D. D.; Vereecken, P.; Ameloot, R. Chemical vapour deposition of zeolitic imidazolate framework thin films. *Nat. Mater.* **2016**, *15* (3), 304−310.

(51) Shekhah, O.; Wang, H.; Kowarik, S.; Schreiber, F.; Paulus, M.; Tolan, M.; Sternemann, C.; Evers, F.; Zacher, D.; Fischer, R. A.; Wöll, C. Step-by-step route for the synthesis of metal- organic frameworks. *J. Am. Chem. Soc.* **2007**, *129* (49), 15118−15119.

(52) Virmani, E.; Rotter, J. M.; Mähringer, A.; Von Zons, T.; Godt, A.; Bein, T.; Wuttke, S.; Medina, D. D. On-surface synthesis of highly oriented thin metal-organic framework films through vapor-assisted conversion. *J. Am. Chem. Soc.* **2018**, *140* (14), 4812−4819.

(53) Lee, J. H.; Kim, D.; Shin, H.; Yoo, S. J.; Kwon, H. T.; Kim, J. Zeolitic imidazolate framework ZIF-8 films by ZnO to ZIF-8 conversion and their usage as seed layers for propylene-selective ZIF-8 membranes. *J. Ind. Eng. Chem.* **2019**, *72*, 374−379.

(54) Wang, X.; Liu, J.; Leong, S.; Lin, X.; Wei, J.; Kong, B.; Xu, Y.; Low, Z.-X.; Yao, J.; Wang, H. Rapid construction of ZnO@ ZIF-8 heterostructures with size-selective photocatalysis properties. *ACS Appl. Mater. Interfaces* **2016**, *8* (14), 9080−9087.

(55) Keum, C.; Lee, H.; Kwon, C.; Han, B.; Lee, S.-Y. Metal-induced self-assembly template for controlled growth of ZIF-8 nanorods. *Chem. Mater.* **2020**, *32* (18), 7941−7950.

(56) Kwon, O.; Kim, M.; Choi, E.; Bae, J. H.; Yoo, S.; Won, J. C.; Kim, Y. H.; Shin, J. H.; Lee, J. S.; Kim, D. W. High-aspect ratio zeolitic imidazolate framework (ZIF) nanoplates for hydrocarbon separation membranes. *Sci. Adv.* **2022**, *8* (1), No. eabl6841.

(57) Moghadam, F.; Lee, T. H.; Park, I.; Park, H. B. Thermally annealed polyimide-based mixed matrix membrane containing ZIF-67 decorated porous graphene oxide nanosheets with enhanced propylene/propane selectivity. *J. Membr. Sci.* **2020**, *603*, 118019.

(58) Kim, D. W.; Han, H.; Kim, H.; Guo, X.; Tsapatsis, M. Preparation of a graphene oxide/faujasite composite adsorbent. *Microporous Mesoporous Mater.* **2018**, *268*, 243−250.

(59) Choi, E.; Hong, S. J.; Kim, Y.-J.; Choi, S. E.; Choi, Y.; Kim, J. H.; Kang, J.; Kwon, O.; Eum, K.; Han, B.; Kim, D. W. Pore tuning of metal-organic framework membrane anchored on graphene-oxide nano-ribbon. *Adv. Funct. Mater.* **2021**, *31* (17), 2011146.

(60) Knebel, A.; Bavykina, A.; Datta, S. J.; Sundermann, L.; Garzon-Tovar, L.; Lebedev, Y.; Durini, S.; Ahmad, R.; Kozlov, S. M.; Shterk, G.; et al. Solution processable metal-organic frameworks for mixed matrix membranes using porous liquids. *Nat. Mater.* **2020**, *19* (12), 1346−1353.

(61) Xia, Y.; Cao, H.; Xu, F.; Chen, Y.; Xia, Y.; Zhang, D.; Dai, L.; Qu, K.; Lian, C.; Huang, K.; et al. Polymeric membranes with aligned zeolite nanosheets for sustainable energy storage. *Nat. Sustainability* **2022**, *5* (12), 1080−1091.

(62) Abdul Hamid, M. R.; Qian, Y.; Wei, R.; Li, Z.; Pan, Y.; Lai, Z.; Jeong, H.-K. Polycrystalline metal-organic framework (MOF) membranes for molecular separations: Engineering prospects and challenges. *J. Membr. Sci.* **2021**, *640*, 119802.

(63) Choi, E.; Hong, S. J.; Chen, J.; Kim, Y. J.; Choi, Y.; Kwon, O.; Eum, K.; Choi, J. I.; Jang, S. S.; Han, B.; Kim, D. W. CO_2-selective zeolitic imidazolate framework membrane on graphene oxide nanoribbons: experimental and theoretical studies. *J. Mater. Chem. A* **2021**, *9* (45), 25595−25602.

(64) Choi, E.; Choi, J. I.; Kim, Y. J.; Kim, Y. J.; Eum, K.; Choi, Y.; Kwon, O.; Kim, M.; Choi, W.; Ji, H.; et al. Graphene nanoribbon hybridization of zeolitic imidazolate framework membranes for intrinsic molecular separation. *Angew. Chem., Int. Ed.* **2022**, *61* (49), No. e202214269.

(65) Gou, Y.; Xiao, L.; Yang, Y.; Guo, X.; Zhang, F.; Zhu, W.; Xiao, Q. Incorporation of open-pore MFI zeolite nanosheets in polydimethylsiloxane (PDMS) to isomer-selective mixed matrix membranes. *Microporous Mesoporous Mater.* **2021**, *315*, 110930.

(66) Dakhchoune, M.; Villalobos, L. F.; Semino, R.; Liu, L.; Rezaei, M.; Schouwink, P.; Avalos, C. E.; Baade, P.; Wood, V.; Han, Y.; et al. Gas-sieving zeolitic membranes fabricated by condensation of precursor nanosheets. *Nat. Mater.* **2021**, *20* (3), 362−369.

(67) Evans, J. D.; Coudert, F.-X. Predicting the mechanical properties of zeolite frameworks by machine learning. *Chem. Mater.* **2017**, *29* (18), 7833−7839.

(68) Wang, Z.; Lobo, R. F.; Lambros, J. The mechanical properties of siliceous ZSM-5 (MFI) crystals. *Microporous Mesoporous Mater.* **2003**, *57* (1), 1−7.

(69) Tan, X.; Robijns, S.; Thür, R.; Ke, Q.; De Witte, N.; Lamaire, A.; Li, Y.; Aslam, I.; Van Havere, D.; Donckels, T.; et al. Truly combining the advantages of polymeric and zeolite membranes for gas separations. *Science* **2022**, *378* (6625), 1189−1194.

(70) Wang, Q.; Jia, D.; Pei, X.; Wu, X.; Xu, F.; Ye, Z.; Wang, H. Mechanical performance of graphenex/poly (ether ketone ketone) composite sheets by hot pressing. *Sci. Rep.* **2022**, *12* (1), 4114.

(71) Igwe Idumah, C.; Okonkwo, U.C.; Obele, C.M. Recently emerging advancements in montmorillonite polymeric nanoarchitectures and applications. *Clean. Mater.* **2022**, *4*, 100071.

(72) Kim, H.; Kim, D. W.; Vasagar, V.; Ha, H.; Nazarenko, S.; Ellison, C. J. Polydopamine-graphene oxide flame retardant nanocoatings applied via an aqueous liquid crystalline scaffold. *Adv. Funct. Mater.* **2018**, *28* (39), 1803172.

(73) Zandiatashbar, A.; Lee, G.-H.; An, S. J.; Lee, S.; Mathew, N.; Terrones, M.; Hayashi, T.; Picu, C. R.; Hone, J.; Koratkar, N. Effect of defects on the intrinsic strength and stiffness of graphene. *Nat. Commun.* **2014**, *5* (1), 3186.

(74) de Oliveira, R. B.; Borges, D. D.; Machado, L. D. Mechanical and gas adsorption properties of graphene and graphynes under biaxial strain. *Sci. Rep.* **2022**, *12* (1), 22393.

(75) Makke, A.; Perez, M.; Lame, O.; Barrat, J.-L. Mechanical testing of glassy and rubbery polymers in numerical simulations: Role of boundary conditions in tensile stress experiments. *J. Chem. Phys.* **2009**, *131* (1), 014904.

(76) Vinh-Thang, H.; Kaliaguine, S. Predictive models for mixed-matrix membrane performance: a review. *Chem. Rev.* **2013**, *113* (7), 4980−5028.

(77) Cussler, E. Membranes containing selective flakes. *J. Membr. Sci.* **1990**, *52* (3), 275−288.

(78) Sheffel, J. A.; Tsapatsis, M. A model for the performance of microporous mixed matrix membranes with oriented selective flakes. *J. Membr. Sci.* **2007**, *295* (1−2), 50−70.

(79) Agrawal, K. V.; Topuz, B.; Pham, T. C. T.; Nguyen, T. H.; Sauer, N.; Rangnekar, N.; Zhang, H.; Narasimharao, K.; Basahel, S. N.; Francis, L. F.; et al. Oriented MFI membranes by gel-less secondary growth of sub-100 nm MFI-nanosheet seed layers. *Adv. Mater.* **2015**, *27* (21), 3243−3249.

(80) Kwon, O.; Choi, Y.; Choi, E.; Kim, M.; Woo, Y. C.; Kim, D. W. Fabrication techniques for graphene oxide-based molecular separation membranes: Towards industrial application. *Nanomaterials* **2021**, *11* (3), 757.